# Density of atoms in Ar*(3p5 4s) states and gas temperatures in an argon surfatron plasma measured by tunable laser spectroscopy

# Density of atoms in Ar*(3p54s) states and gas temperatures in an argon surfatron plasma measured by tunable laser spectroscopy

S. Hübner, N. Sadeghi, E. A. D. Carbone, and J. J. A. M. van der Mullen

Citation: J. Appl. Phys. **113**, 143306 (2013); doi: 10.1063/1.4799152
View online: http://dx.doi.org/10.1063/1.4799152
View Table of Contents: http://jap.aip.org/resource/1/JAPIAU/v113/i14
Published by the American Institute of Physics.

JOURNAL OF APPLIED PHYSICS **113**, 143306 (2013)

# Density of atoms in Ar*($3p^5 4s$) states and gas temperatures in an argon surfatron plasma measured by tunable laser spectroscopy

S. Hübner,[1,a)] N. Sadeghi,[2] E. A. D. Carbone,[1] and J. J. A. M. van der Mullen[1]
[1]*Department of Applied Physics, Eindhoven University of Technology, P.O. Box 513, 5600MB Eindhoven, The Netherlands*
[2]*LIPhy, Université Joseph Fourier & CNRS, UMR 5588, Grenoble F-38041, France*

(Received 18 February 2013; accepted 19 March 2013; published online 10 April 2013)

This study presents the absolute argon 1 s (in Paschens's notation) densities and the gas temperature, $T_g$, obtained in a surfatron plasma in the pressure range $0.65 < p < 100$ mbar. The absorption signals of 772.38, 772.42, 810.37, and 811.53 nm lines, absorbed by atoms in $1s_3$, $1s_4$, and $1s_5$ states, were recorded with two tunable diode lasers. $T_g$ is deduced from the absorption line shapes when scanning the laser wavelengths. The line profile, which is a Doppler broadening dominated Gaussian at gas pressures of $p < 10$ mbar, changes to a Voigt shape at $p > 10$ mbar, for which the pressure broadening can no more be neglected. $T_g$ is in the range of 480-750 K, increasing with pressure and decreasing with the distance from the microwave launcher. Taking into account the line of sight effects of the absorption measurements, a good agreement is found with our previous measurements by Rayleigh scattering of $T_g$ at the tube center. In the studied pressure range, the Ar(4 s) atom densities are in the order of $10^{16} - 10^{18}$ m$^{-3}$, increasing towards the end of the plasma column, decreasing with the pressure. In the low pressure side, a broad minimum is found around $10 < p < 20$ mbar and hence the Ar(4 s) atom densities increase slightly with rising pressure. For the studied pressure range and all axial positions, the density ratio: $1s_5/1s_4/1s_3$ is very close to a Boltzmann equilibrium by electron impact mixing at the local $T_e$, which was previously measured by Thomson scattering. The Ar(4 s) densities are successfully compared to a detailed Collisional Radiative Model. © *2013 American Institute of Physics*. [http://dx.doi.org/10.1063/1.4799152]

## I. INTRODUCTION

The argon atoms excited into the 4 s level-group are often the most abundant energy carrying atoms in argon plasmas. This 4 s group is the lowest block of excited states and consists of two resonant and two metastable levels. Of these four levels especially the metastable levels get a lot of attention. This is attributed to their long life time. However, in plasmas of which *pd*, the product of pressure and size, is not too small, the resonant 4 s levels might have a high density as well. The reason is that resonant radiation is easily trapped. So the photons created in the decay of resonant Ar(4 s) levels at a certain location are immediately reabsorbed in adjacent positions. Especially in plasmas generated at high mean electron energy and low electron densities, the density of 4 s levels can be even higher than that of the ions. The design of remote plasma applications is usually based on this trend. The efflux of Ar(4 s) from the plasma can be used for excimer formation[1] or to generate active species for various applications,[2–4] e.g., by excitation transfer to $N_2$[5] or by Penning ionization.[6]

The argon 4 s group is an important step in the ionization mechanism when direct ionization is too slow. For plasmas with low electron temperature (1 eV), the ionization is mainly provided by the ladder-climbing ionization mechanism; the creation of Ar(4 s) is followed by transitions from 4 s to, e.g., 4 p, 3 d, 4f, etc., up to ionization. Also, collision between two metastable atoms can partially contribute to the ionization. Thus, Ar(4 s) plays a crucial role in plasma creation. Therefore, the insight in the kinetics of Ar plasmas must be based on a proper knowledge of the number densities and the rates of creation and destruction of atoms in Ar(4 s) levels.

To determine the absolute number densities of Ar atoms in the 4 s levels, optical absorption spectroscopy on Ar(4 p)-Ar(4 s) transitions is the most appropriate method. In fact, the optical emission is forbidden from $1s_5$ and $1s_3$ metastable states and is hardly applicable for the $1s_4$ and $1s_2$ resonance states with their transition wavelength of around 100 nm. Moreover, this emission is very often trapped. Several absorption techniques exist. One can use *passive spectroscopy* by studying the self-absorption of the photons generated in 4 p-4 s transitions. By using line intensity ratios of different 4 p-4 s transitions under certain conditions, one can determine the escape factors and from that the density of the absorber, Ar(4 s).[7,8]

The other route is that of *active spectroscopy* in which an external radiation source is used to study how the beam generated by that source is absorbed by the plasma. For that, three different types of sources can be used: a spectral broad band source providing a quasi continuum,[9,10] an atomic transition source, delivered by another Ar plasma[11,12] or narrow band sources given by tunable lasers.

This study is based on the latter method using a narrow band tunable diode lasers (TDL) source. This has the advantage that apart from the densities of the absorbing atoms, one

a)Electronic address: S.Huebner@tue.nl

 

can also determine the line shape of the transitions. As the latter depends on the Doppler effect and on other broadening mechanisms, it gives additional insight into the plasma. Nowadays, this is a well-known technique used by many groups on various plasma sources.[13–17]

The method is based on scanning the wavelength of the TDL probe laser across the atomic line shape. This procedure is demanding in terms of (laser) equipment but the detected density of the absorbing level is in principle independent of the line shape. For that, the laser has to be stable and its line width $\Delta\nu_{\text{laser}}$ must be much smaller than the spectral width of the atomic transition $\Delta\nu_{2p-1s}$. For our study, we can write

$$\Delta\nu_{\text{laser}} < 10\ \text{MHz} \ll \Delta\nu_{2p-1s} \approx 1\,\text{GHz},$$

meaning that the line widths of our lasers are small enough to investigate in detail the line shape of the transitions.

In order to get insight in plasma kinetics, we need a stable, reliable, and adjustable plasma source. For this, we selected a microwave driven surface wave discharge, launched by a surfatron. The pressure range of this surfatron plasma is large (0.1 millibar-1 atm) and the plasma source allows a (quite) independent tuning of the electron density ($n_e$) while maintaining the electron temperature ($T_e$) to more or less the same value.[18–20] In the past, the surfatron plasma was subjected to absorption spectroscopy and models were employed in order to determine the density of the Ar(4 s) states together with that of other levels.[8,21]

In this study, we use two different diode lasers covering the transitions $2p_2$-$1s_3$, $2p_7$-$1s_5$, $2p_7$-$1s_4$, and $2p_9$-$1s_5$ so that the densities of the $1s_3$, $1s_4$, and $1s_5$ could be probed. As the logarithm of the absorption signal is linearly related to the absorber density, we obtain absolute densities of the Ar(4 s) atoms. Our results were compared to a collisional radiative model (CRM) containing 80 levels and their respective transitions probabilities.[22] With Ar(4 s) atoms at hand, the main plasma parameters like the electron density $n_e$ and temperature $T_e$ well-known from our previous Thomson scattering experiments and the gas temperature deduced from the present work and our previous Rayleigh scattering measurements,[23] we get by means of the comparison of the measured and modelled densities a good picture of the plasma kinetics.

## II. THEORY

### A. Laser photon absorption

The transport of a laser beam through a plasma is described by Beer-Lambert's law

$$\frac{dI_\nu(\nu,x)}{dx} = -k(\nu,x)I_\nu(\nu,x) \tag{1}$$

that shows how the intensity $I_\nu(\nu)$ in units $\text{Wm}^{-2}\,\text{sr}^{-1}\,\text{Hz}^{1}$ of the beam changes along its path through the plasma due to absorption. $k(\nu)$ (in $\text{m}^{-1}$) is known as the local *absorption* coefficient

$$k(\nu) = [\lambda^2/(8\pi)][\eta(l) - \eta(u)]g(u)A(u,l)\phi_\nu(\nu)$$

that can best be denoted by the *total* absorption coefficient as it is composed of two terms, one from the lower (l) and the other from the upper (u) level. The first gives the coefficient for *pure absorption*, the second for *stimulated emission*. Here, A(u,l) is the Einstein coefficient of the transition, $\phi_\nu(\nu)$ the line profile while $\eta = n/g$ refers to the level density per number of states; $n$ is the level density and $g$ the degeneracy. In our plasma conditions, we will find $\eta(l)/\eta(u) \approx 10^2 - 10^3$ so that we can safely ignore the stimulated emission and write:

$$k(\nu) = (\lambda^2/8\pi)n(l)g(u)/g(l)A(u,l)\phi_\nu(\nu). \tag{2}$$

Rearranging terms and integrating the result over the line of sight gives

$$\begin{aligned}\mathcal{A}(\nu) &= Ln[I_\nu(\nu,0)/I_\nu(\nu,L)] \\ &= (\lambda^2/8\pi)g(u)/g(l)A(u,l)\int_0^L n(l,x)\phi_\nu(\nu)dx,\end{aligned} \tag{3}$$

where L is the length of the plasma-laser intersection region and $\mathcal{A}(\nu)$ is the spectral absorbance. Subsequently, the integral over the line shape $\phi_\nu(\nu)$ gives

$$\begin{aligned}S &= \int_{-\infty}^{+\infty}\mathcal{A}(v)d\nu \\ &= (\lambda^2/8\pi)g(u)/g(l)A(u,l)\int_{-\infty}^{+\infty}\int_0^L n(l,x)\phi_\nu(\nu)dxd\nu.\end{aligned} \tag{4}$$

That can be made more comprehensive by equating the combined transition and line of sight integral $S$, by writing $\int_\nu\int_x^L n(l,x)\phi_\nu(\nu)dxd\nu \equiv \langle n(l)\rangle L$. With this, Eq. (4) can be written as

$$\langle n(l)\rangle = \frac{8\pi S}{\lambda^2}\frac{g(l)}{g(u)}\frac{1}{A(u,l)L}. \tag{5}$$

### B. Practical formulas

By rewriting Eq. (5), we can determine the absorber densities from $S$ [Hz] and $L$ [m] via

$$n(l) = \frac{C(u,l)S}{L},$$

where $C(u,l) = 8\pi\lambda^{-2}g(l)/g(u)A(u,l)^{-1}$. The numerical value of $C$ is given in Table I together with other transition specific quantities for the relevant transitions.

### C. Line shape

By scanning the laser wavelength across the atomic line profile, we not only deduce the peak absorbance but also the line shape that gives insight in the line broadening mechanisms. Using the formulas given in Refs. 24 and 25, we find for our plasma conditions for the natural and Stark broadening typically $\Delta\nu_{\text{nat}} < 6\,\text{MHz}$ and $\Delta\nu_{\text{Stark}} < 50\,\text{MHz}$, which

TABLE I. Summary of transition quantities used in this study.

| $l$ | $u$ | Wavelength (nm) | $A$ (Hz) | $g(l)/g(u)$ | $C(u,l)$ (s m$^{-2}$) |
|---|---|---|---|---|---|
| $1s_3$ | $2p_2$ | 772.42 | $1.17 \times 10^7$ | 1/3 | $1.20 \times 10^6$ |
| $1s_5$ | $2p_7$ | 772.38 | $5.18 \times 10^6$ | 5/3 | $1.36 \times 10^7$ |
| $1s_4$ | $2p_7$ | 810.37 | $2.5 \times 10^7$ | 3/3 | $1.53 \times 10^6$ |
| $1s_5$ | $2p_9$ | 811.53 | $3.31 \times 10^7$ | 5/7 | $8.24 \times 10^5$ |

can be neglected with respect to the Doppler width. Under our experimental conditions, this is in the range of $\Delta\nu_{\text{Doppler}} \approx 1$ GHz. At low pressure, when a pure Doppler profile can be assumed, the line profile has a Gaussian shape, for which the width reads

$$\Delta\nu_{\text{Doppler}}(\text{FWHM}) = 7.16\,10^{-7}\nu(T_g/M)^{1/2}(\text{Hz}),$$

where $T_g$ is the gas temperature (K), M the atom mass (amu), and $\nu$ the corresponding transition frequency (Hz). For argon atoms, this can be rearranged giving the gas temperature via

$$T_g = 7.8\,10^{13}(\Delta\nu_{\text{Doppler}}/\nu)^2(\text{K}). \quad (6)$$

Apart from Doppler broadening, at pressures over tens of millibars one should also consider van der Waals and Resonance broadening for lines absorbed by atoms in the metastable ($1s_5$ and $1s_3$) and resonance ($1s_4$) states, respectively. That leads to a Voigt profile with a Lorentzian component and a slight shift of the line center. The pressure broadening depends on the gas temperature $T_g$, and using coefficients reported in the literature for the Van de Waals broadening,[26,27] we write for the width of the corresponding lines landing on metastable states (811.53, 772.38, and 772.42 nm lines)

$$\Delta\nu_{\text{VdW}}(\text{FWHM}) = Kp(300/T_g)^{0.7}(\text{Hz}), \quad (7)$$

where $p$ (millibar) is the gas pressure and the constant $K$ has the values $1.4\,10^7$, $1.3\,10^7$, and $2.0\,10^7$ Hz for the 811.53, 772.38, and 772.42 nm lines, respectively. For the 810.37 nm line which ends on a resonant state, we write with the resonance broadening coefficient reported by[28]

$$\Delta\nu_{\text{R}}(\text{FWHM}) \approx 3.2\,10^7 p(300/T_g)(\text{Hz}). \quad (8)$$

Since $T_g$ enters in both the Doppler and the pressure broadening, it will act as the only free parameter for the line shape of the Voigt fit. The basic assumption we are making on the equality of the kinetic energy (temperature) of argon atoms in the ground state and in Ar(4 s) states, monitored by laser absorption, is justified by following facts. First, these states are mainly populated by electron impact from the ground state, during which the kinetic energy of the atom should not be significantly modified. Also, due to the radiation trapping, atoms in the $1s_2$ and $1s_4$ resonance states are continuously exchanged with ground state atoms within a few ns. Finally, the cross section for elastic collision and metastability exchange between Ar atoms and atoms in the $1s_3$ and $1s_5$ metastable states is about $10^{-18}$ m$^2$. At 1 millibar, this leads to a collision frequency of about $10^7$ s$^{-1}$, much faster than the loss frequency of metastable atoms (for more detail see, e.g., Ref. 29). In conclusion, under our experimental condition, the velocity distribution of Ar atoms in ground and excited states is identical and absorption profiles from Ar(4 s) states provide the $T_g$ value.

## III. EXPERIMENTAL SETUP AND PROCEDURE

### A. Setup

The plasma under study is a microwave-induced surface wave discharge (surfatron plasma) driven at 2.45 GHz (Fig. 1). The discharge is confined in a quartz tube with 6 mm inner (8 mm outer) diameter. Due to the high electron density, the central part of the plasma in the tube becomes opaque for the $\mu$-wave field. Consequently, a surface wave can propagate at the quartz-plasma interface. This wave provides a power input for the plasma which leads to an extension of the plasma column along the tube. It was shown that in the low pressure range, the absorbed power of the surface wave provides an almost linear decreasing electron density along the column, while the electron temperature remains rather constant in the whole plasma. The inlet argon gas used in our experiments is 99.999% pure and the working pressures are 0.65–105 millibars. More details can be found in Refs. 18, 19, and 30.

Two external cavity laser diodes are used to determine the absorption line profiles. Absolute densities of atoms in these 1 s states and the gas temperature can be deduced from these absorption profiles. The laser TDL-1 (Littman configuration, TEC 500; Sacher Lasertechnik) can be tuned on the 772.38 nm and 772.42 nm argon lines to probe metastable

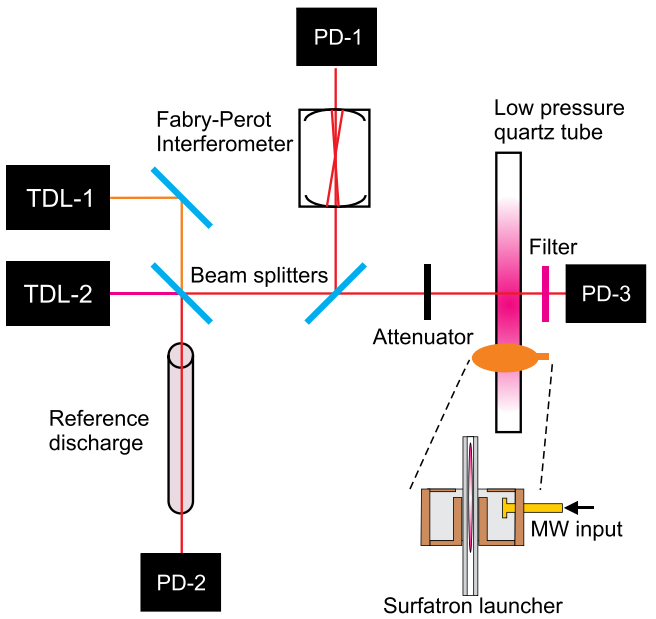


FIG. 1. Scheme of the experimental setup. Two TDLs are combined and pass the plasma column perpendicular to the axis. The plasma tube can be moved with respect to the laser beams. Data collection system and vacuum equipment are not shown for clarity.

atoms in $1s_5$ and $1s_3$ states, respectively. TDL-2 (Littrow configuration, DL100, Toptica) can be tuned on the argon lines 810.37 nm and 811.53 nm to probe atoms in the resonant $1s_4$ and metastable $1s_5$ states, respectively. The coarse wavelength adjustment is obtained by moving the grating angle and diode's current and temperature. The laser wavelength can be then finely tuned across the absorption line (about 8 GHz mode-hop free) by slightly tilting the cavity mirror (TDL-1) or the grating (TDL-2) with a piezoelectric device. The beams of both diode lasers are combined by a beam splitter. A 2nd beam splitter provides a secondary beam which is used for the frequency calibration of the TDLs. The combined laser beam is sent across the centre of the plasma tube and then detected by a photodiode (PD-3) backed up by a $10^6$ V/A transimpedance amplifier. At the plasma tube position, the beam diameter is about 1 mm. For the reduction of unwanted plasma emission a band-pass filter ($\sim$10 nm FWHM, centred at 780 or 805 nm) is placed in front of PD-3. Moreover, to avoid optical pumping and render the laser non-intrusive,[31] the beam is attenuated to less than 1 $\mu$W. To calibrate the frequency shift of the TDLs while scanning, a part of the secondary beam crosses a 25 cm long confocal Fabry-Perot-Interferometer (FPI) and is detected by PD-1. The 0.300 GHz intervals between peaks of the transmitted intensity by the FPI (its free spectral range, FSR) provide the precise relative frequency shifts. Another part of the beam is sent into a low pressure argon glow discharge reference cell and is detected by PD-2. The absorption signal from this later helps for setting the TDLs around the wavelengths used in this study.

The absorption signals from the plasma and the reference cell together with the signal from the FPI are simultaneously recorded and averaged over 50–400 scans of the laser by a digital oscilloscope (Lecroy Waverunner).

### B. Data treatment

One of the aims of the experimental procedure is to determine the spectral absorption area S (see Eq. (4)) the other being the determination of the gas temperature from the spectral line shape. For both objectives, we need to determine the frequency dependent intensity of the four recorded signals. This is illustrated in Figure 2. With laser on, the spectral intensities $I_\nu(\nu, \text{off})$ and $I_\nu(\nu, \text{on})$ are recorded by scanning the TDL when the plasma is off and on, respectively. With TDL off, $I_{\text{back}}(\nu)$ and $I_{\text{plasma}}(\nu)$ are recorded without and with plasma, respectively. So the spectral dependent absorbance[32] is given by Eq. (3)

$$\mathcal{A}(\nu) = Ln\left(\frac{I_\nu(\nu,0)}{I_\nu(\nu,L)}\right) = Ln\left(\frac{I_\nu(\nu,\text{off}) - I_{\text{back}}(\nu)}{I_\nu(\nu,\text{on}) - I_{\text{plasma}}(\nu)}\right). \quad (9)$$

The averaged Ar(4 s) densities across the diameter are obtained using Eqs. (4) and (5) as described in Sec. II. The gas temperature is deduced by fitting the spectral profile of $\mathcal{A}(\nu)$ with a Gaussian or Voigt function. Examples are given in Figures 3(a) and 3(b) for the absorption spectra of 772.43 and 811.53 nm line recorded at 0.65 and 105 millibars, respectively. Note that we neglect in our fitting procedure the small line shift.

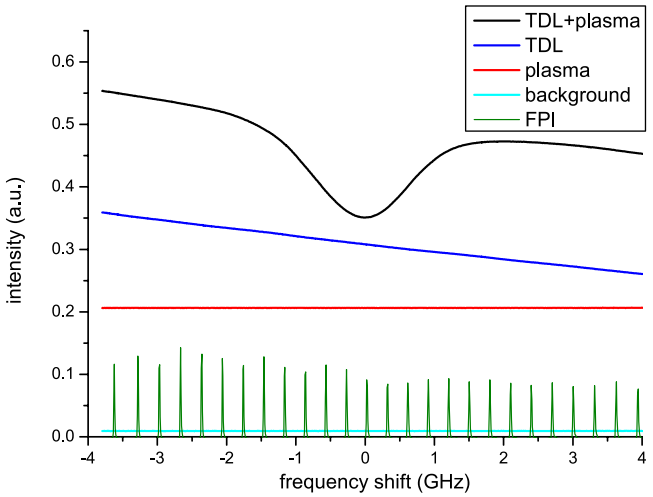


FIG. 2. Measurement procedure, recorded is the laser light with and without plasma, plasma light and background. Moreover the calibration signal from the Interferometer with the FSR of 0.3 GHz is shown. Experimental conditions are: 811.5 nm line; p = 80 millibars; z = 2 cm; 68 W input $\mu$-wave power.

## IV. RESULTS AND DISCUSSION

For argon pressures ranging from 0.65 to 105 millibars, absorption profiles from all three $1s_3$, $1s_4$, and $1s_5$ states were recorded along the plasma column at different axial distances from the launcher. Special care had to be taken for the plasma reproducibility; this was done by taking the plasma column length as a reference; a drift in plasma conditions manifests in the plasma length. Once calibrated in the frequency scale by using the F-P peaks, these profiles have been fitted with Gaussian and Voigt functions, respectively. Fitting parameters provide the gas temperature and the absolute averaged density of the absorbing atoms. Results for the gas temperature and Ar(4 s) density are presented and discussed in subsections IV A, IV B and IV C, IV D, respectively.

### A. Gas temperature

As shown in Fig. 3, and Sec. III, the gas temperature can be deduced from the shape of the absorption profile. For the low pressure range, we can use the Gaussian formula of Eq. (6). Above 10 millibars, the pressure broadening is not any longer negligible and a Voigt fitting procedure is used, based on Eq. (6) and (7) or (8). Results for different pressures and axial positions are shown in Figure 4. $T_g$ is higher with increasing pressure and it slightly decreases with the distance from the microwave launcher. It is also apparent that higher pressure leads to larger uncertainties on the $T_g$ data.

For the low pressure range, the quality of the line profile fitting is very good and it is self-consistent in the sense that the $T_g$ values deduced from the fitting of different lines agree well. As an example, for 0.65 millibars, the deviations are below 3%. But the fitting of the absorption signal for higher pressures seems to be less precise. Larger discrepancies between results from different lines are found at pressures ranging from 20 to 105 millibars. To deduce a mean gas temperature, we average the $T_g$ values deduced from different

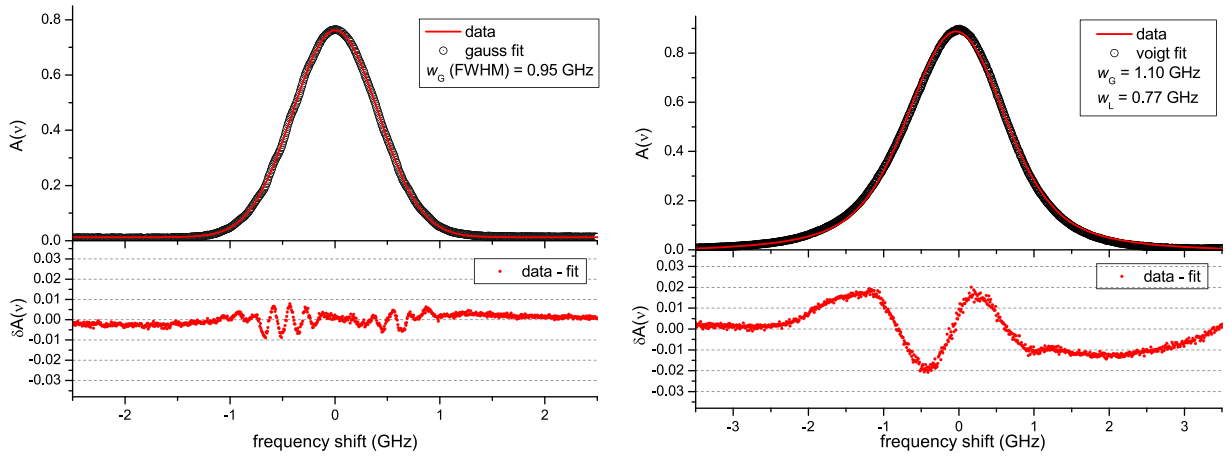


FIG. 3. Top: plot of absorbance $\mathcal{A}(\nu)$ versus frequency shift for: (a) 772.43 nm line at 0.65 millibars, fitted by a Gaussian function; (b) for 811.53 nm line at 105 millibars, fitted with a Voigt function. By the residue given below, it is clear that a good fit is obtained for 0.65 millibars, while at 105 millibars higher residues are present.

lines and use their range of difference as an indication for the error bar, which reaches 12% for 105 millibar.

This large uncertainty in the high pressure range is partly because we are assuming a perfectly radially homogeneous $T_g$, which cannot be entirely correct. In fact, we suppose an identical absorption line profile all along the absorption length; i.e., the same $T_g$ and Ar atom density at a fixed axial position. But in the presence of a radial temperature gradient, the Gaussian ($W_G$) and Lorentzian ($W_L$) components of the Voigt profile will change with the radial position and thus the resulting line shape, obtained by their averaging along the diameter of the plasma tube, will not have a perfect Voigt profile. So, fitting the experimental profiles with a Voigt function, in which $W_G$ and $W_L$ are linked to each other by a single $T_g$ can induce an error with large residual. We also cannot exclude a small influence of the plasma on the laser frequency, which means that $I_\nu(0)$ can be slightly different between plasma on and off. This can introduce a small inaccuracy on the determination of $\mathcal{A}(\nu)$ and thus the $T_g$. Another error source could be the inaccuracy of some of the pressure broadening coefficients of absorption lines, listed in Sec. II C. These coefficients being often obtained from the emission line profiles in thermal plasmas in which $T_g$ and the uncertainty on it are usually very large. Finally, it should be stressed that with about 8 GHz mode-hop free scan of the TDLs, the far wings of the Lorentzian part of the line profile might not be covered completely.

### B. Comparison of gas temperature

In order to compare the present results on the gas temperature, a comparison is made in Figure 5 with our earlier measurements by Rayleigh laser scattering (RyS), carried out in the same plasma tube and under similar conditions.[23] However, one should keep in mind that there are essential differences in these two methods. RyS measures the ground state Ar density at the plasma tube axis, from which using

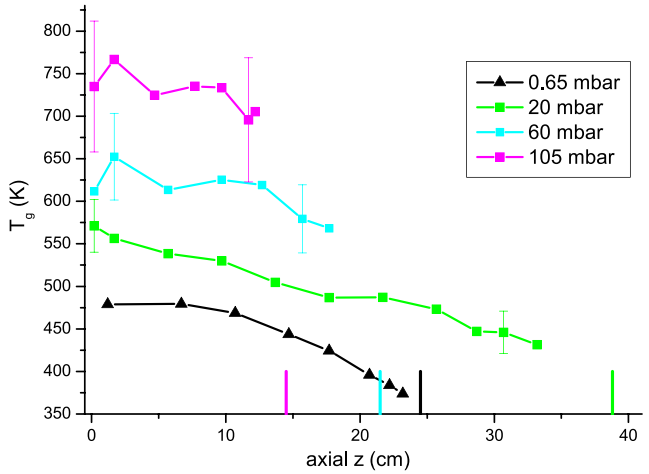


FIG. 4. $T_g$ as a function of axial position for different gas pressures. The error bars are decreasing with lower pressure down to 0.65 mbar where the error indication is smaller than the symbol size. For each pressure, the end of the plasma column is indicated by a vertical line.

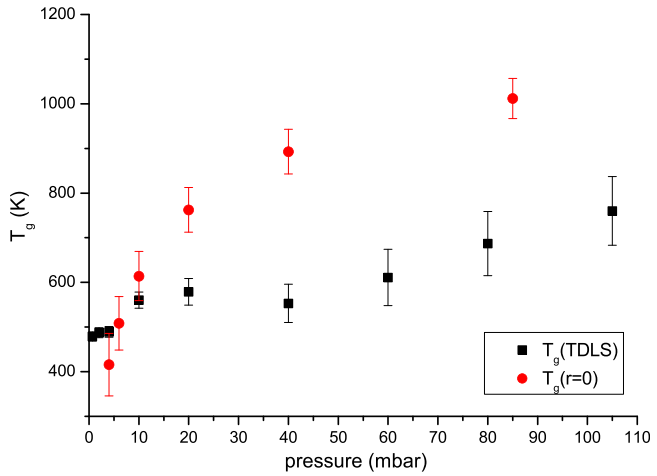


FIG. 5. $T_g$ at the launcher position for different pressures from this experiment (full squares) and measured as described in Ref. 23 by Rayleigh scattering (circles).

the ideal gas law $T_g(r = 0)$ is obtained. On the other side, TDL spectroscopy provides a line of sight averaged absorption line profile from atoms in a certain Ar(4 s) state, from which $T_g$ is obtained.

As mentioned before, higher pressure leads to higher $T_g$. That can also be predicted by the fact that the dominant heating mechanism is the elastic electron-heavy particle collisions, while the heat is lost to the wall by conductive transport. This was already observed and discussed.[23]

### C. Densities of Ar(4 s) atoms

For argon pressures ranging from 0.65 to 105 millibars, the line of sight averaged densities of atoms in $1s_3$, $1s_4$, and $1s_5$ states were measured by TDL spectroscopy for different axial positions along the surfatron plasma column, according to Sec. III. The axial variation of these densities are presented in Figures 6 (p = 0.65, 4, 10 millibars) and 7 (p = 20, 60, 105 millibars). For each pressure, the position of the end of the corresponding plasma column is indicated by a vertical line.

It can be seen that the Ar(4 s) atom densities range between $10^{16}$ and $10^{18}$ $m^{-3}$. Generally speaking, the dependence on gas pressure and axial position of the Ar(4 s) densities are in all three studied states very similar. For lower pressures (0.65–20 millibars) in Figure 6 the densities decrease monotonically with pressure but after having reached a plateau around 10–20 millibars, they increase again at higher pressures (20–105 millibars), as shown in Figure 7. The main underlying phenomenon for this pressure dependence goes along with the continuous enhancement of $n_e$ and decrease of $T_e$ with the gas pressure, as measured in Ref. 19. In the low pressure side, a high $T_e$ favors an efficient excitation of Ar(4 s) states[33] and a low $n_e$ results in a low stepwise ionization of atoms in these states. Both phenomena acting in the same way, the lower the pressure, the higher the Ar(4 s) atom densities are. In the high pressure side, the decrease in excitation rate coefficient with the decrease in $T_e$ is (almost) balanced by the enhancement of both argon atom density in the ground state, $n_a$. But also, increasing $n_a$ accelerates the

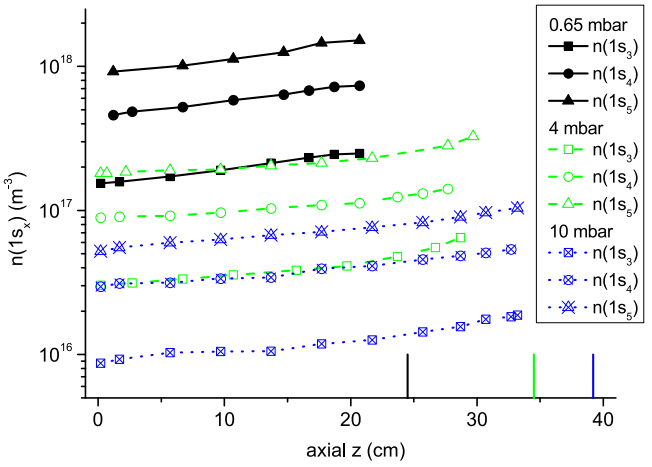


FIG. 6. Absolute $1s_3$, $1s_4$, and $1s_5$ atom densities for gas pressures of 0.65, 4 and 10 millibars along the plasma column. The ends of the plasma columns are indicated by vertical lines.

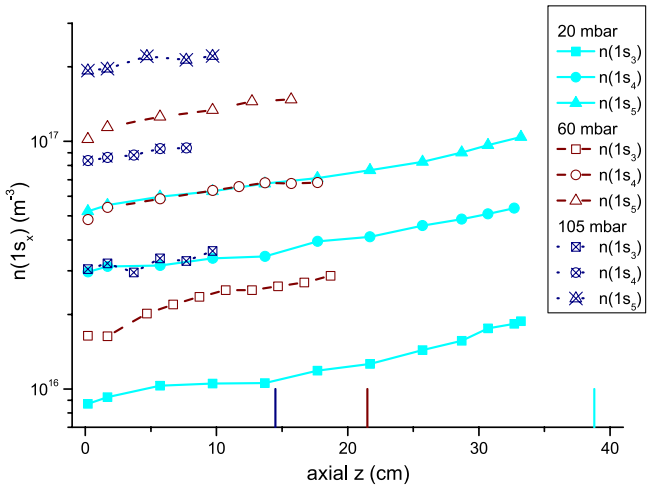


FIG. 7. The same as in Fig. 6 but for gas pressures of 20, 60, and 105 millibars.

conversion of $Ar^+$ ions into $Ar_2^+$ ions by three body reaction.[33,34] The very fast dissociative recombination of these $Ar_2^+$ ions then becomes a new source for the production of atoms in the excited states. As a result, in this regime, the higher the pressure, the higher the Ar(4 s) atom density is.

Figures 6 and 7 also show a monotonic enhancement of Ar(4 s) atoms densities along the plasma column towards the end. Typically, this increase accounts for a factor of 2. However, as shown in Fig. 4, at all studied pressures the gas temperature is decreasing along the plasma column, resulting in an enhancement of the ground state Ar atoms density, $n_a$, according to the ideal gas law. In Figure 8, the evolution along the plasma column of the $n(1s_5)/n_a$ densities ratio is shown. A small rising trend of the density ratio along the plasma column is still present but now it does not exceed a factor of 1.4. Given that at fixed pressure the electron temperature should not significantly change, but $n_e$ should decrease along the plasma column,[20,33] this almost constant $n(1s_5)/n_a$ ratio indicates that the density of atoms in Ar(4 s) states is in electron impact saturation regime; i.e., production of Ar(4 s) by electron impact from the ground state is mainly

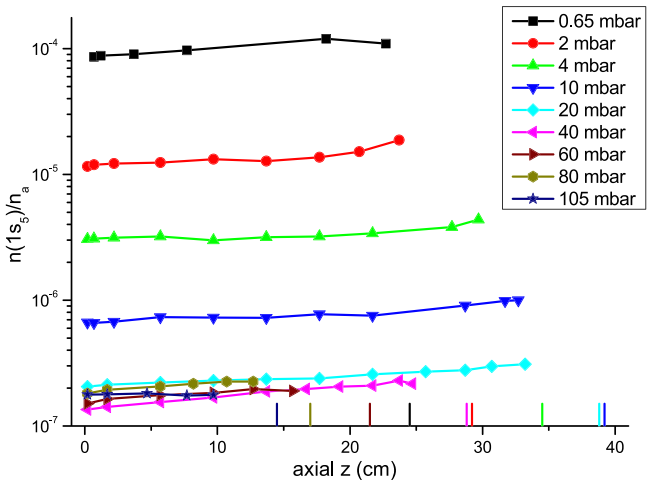


FIG. 8. The $n(1s_5)/n_a$ ratio versus the distance from the launcher, taking the gas temperature into account for the ground state density.

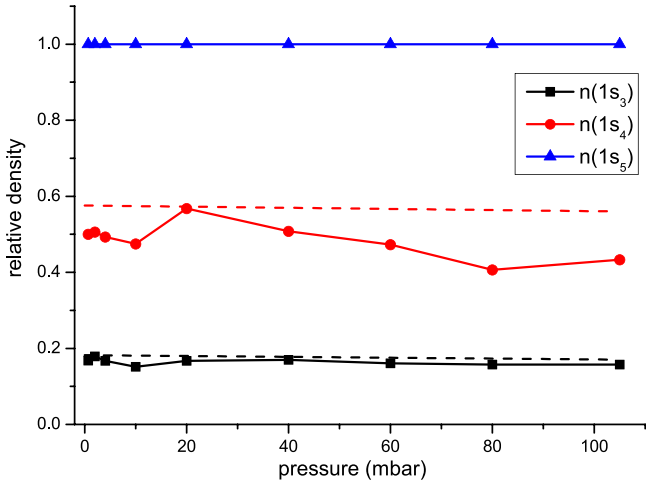


FIG. 9. $n(1s_3)$ and $n(1s_4)$ densities close to the launcher normalized to $n(1s_5)$ from the same position as function of pressure (symbol + lines). Indicated are the densities according to Boltzmann equilibrium and $T_e$(TS) (dashed lines).

balanced by their electron impact ionization. So, the $n(4s)/n_a$ ratio becomes insensitive to the decay of $n_e$ along the plasma column. The decrease of this ratio with increasing pressure up to 20 millibars results from the decay of $T_e$, which lowers more the excitation rate than the ionization rate. Above 20 millibars, the decay with pressure of $T_e$ is much less pronounced[19,20] and also as already mentioned, there can be a contribution from molecular ion recombination to Ar(4 s) atom formation. All these render the $n(1s_5)/n_a$ ratio almost constant above 20 millibars.

Another important point which should be addressed is the population distribution between different levels of the Ar(4 s) manifold. In Figure 9, the relative densities $n(1s_4)/n(1s_5)$ and $n(1s_3)/n(1s_5)$ are reported for different pressures close to the launcher position. We observe that these ratios are almost independent of the pressure, particularly for the $Ar(1s_3)$ state. Assuming that the frequencies of electron impact transfers between the four levels of the Ar(4 s) manifold are high enough to establish a Boltzmann equilibrium between these levels, the density distribution between levels "a" and "b" belonging to this manifold obeys the equation:

$$n(b)/g(b) = n(a)/g(a)\, exp(-E_{ab}/k_B T_e),$$

where $g(i)$ is the statistical weight of the level and $E_{ab}/k_B$ is the energy gap between the levels, which in the present case is less than 0.3 eV. Taking $T_e = 1.4$ eV, as a mean value measured before by Thomson scattering, one ends up with

$$n(1s_2)/n(1s_3)/n(1s_4)/n(1s_5) = 0.49/0.18/0.57/1.$$

In Figure 9, these calculated values for $n(1s_4)/n(1s_5)$ and $n(1s_3)/n(1s_5)$ are also indicated by dashed lines. It can be seen that in this very high electron density plasma, for all pressures the densities of metastable states are in "perfect" Boltzmann equilibrium. This contrasts with what was reported in Ref. 8 for a surfatron plasma with the same radius, in which the $n(1s_3)/n(1s_5)$ ratio was rising from 0.1 at 0.26 millibars to 0.35 at 3.7 millibars. Bakowski *et al.*[35] also reported a density ratio near 0.1 in an ICP plasma source. For the $n(1s_4)/n(1s_5)$ ratio, one observes a small deviation from the predicted statistical equilibrium. This might be related to the radiative escape (despite the radiation trapping) from the resonant $n(1s_4)$ state.

To summarize, we conclude that the internal density distribution within the 4 s group is rather good described by a Boltzmann equilibrium for the experimental range of electron density and gas pressure. That allows also to predict the density of the experimentally not accessible $n(1s_2)$. That should be slightly lower than $n(1s_4)$ due to the small difference in their respective energy levels.

### D. Comparison of Ar(4 s) atom densities

In the literature, we could only find one study on the absolute Ar(4 s) populations in an argon surfatron induced plasma, reported by Lao *et al.*[8] In that work, the intensity ratios of 2 p-1 s lines ending in the same $1s_x$ state, where x = 2, 3, 4, or 5, were used to deduce the density of the $1s_x$ state. The authors use the significant self-absorption of strong lines, with oscillator strengths in the range of 0.2–0.5, to calculate the absorber density from their escape factor. For the $1s_5$ level, their data at 0.67 and 3.7 millibars are shown in Figure 10, together with our results at pressures approaching theirs. At 0.65 mbar, a reasonable agreement is found but about a factor of 2 difference exists around 4 millibars.

Apart from a comparison with previous experimental results, we also compared our findings with the outcome of a collisional radiative model (CRM) based on the work of Graef.[22] That model includes about 80 energy levels of argon and incorporates a large number of radiative transitions and collisional transfers between these levels. The electron impact transfer rates have been determined using cross sections from empirical (ground to 4 s, 4 p, 3 d, 5 s, and 5 p levels), calculated (4 s to 4 s, 4 p, 3 d, and 5 s), and semi-empirical (the rest of the system) found in the literature. To determine the rate coefficients of the collisional transfers, the cross sections are convoluted with a Maxwellian EEDF. Radiative transition probabilities are taken from the NIST database.[36] For the resonance lines starting from Ar(4 s)

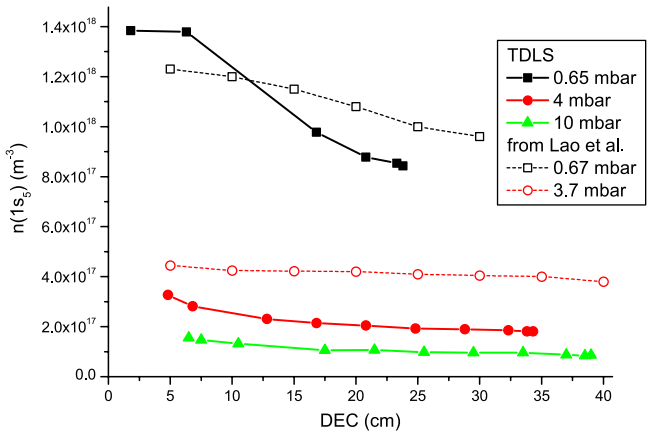


FIG. 10. Comparison of the $n(1s_5)$ with other measurements: TDLS results and data from self-absorption measurements from Ref. 8 as function of the distance to the end of the column (DEC).

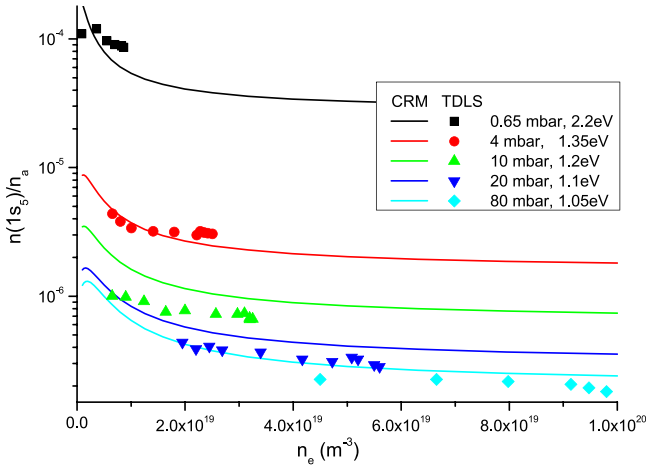


FIG. 11. Comparison of the $n(1s_5)/n_a$ ratio at 5 pressures from the experiments (scatter) with a CRM (line) as a function of $n_e$. Input parameter in the CRM is the experimentally determined, axially constant,[20] $T_e$.

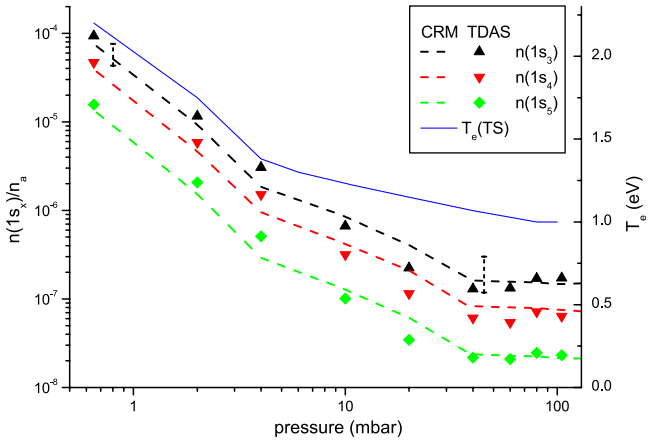


FIG. 12. The measured $n(1s)/n_a$ ratio close to the launcher for different pressures. Comparison is made by means of a full CRM knowing $T_e$ and $n_e$ from Thomson scattering ($T_e$ is shown). For the normalization with respect to $n_a$, the gas temperature is taken from the present work.

states, escape factors can be included in order to take the radiation trapping into account. Additionally, (de)excitation and ionization by heavy particle collisions are included for all levels in the form of empirical rate coefficients.

The input parameters are the atom density $n_a$, and the electron density and temperature, $n_e$ and $T_e$, the latter two are taken from previous experiments by Thomson Scattering, partly unpublished and partly published in Ref. 19.

Figure 11 compares the fractional $n(1s_5)$ density $(= n(1s_5)/n_a)$ calculated by the CRM with those obtained experimentally. A fairly good agreement is observed. The model shows a significant rise of the $n(1s_5)$-fraction for decreasing $n_e$, i.e., approaching the end of the plasma column. But for the experimental data points, the variation with $n_e$ is less pronounced and at a fixed pressure $n(1s)/n_a$ remains almost constant.

The reason for the increase in the model is a Corona case B effect.[37] Since the electron temperature is relatively low, the plasma creation is mainly done by stepwise processes performed by e-impact transitions. In the ladder climbing process, Ar(4 s) is easily excited to higher states provided $n_e$ is high enough. However, at lower $n_e$ values, the overall excitation is obstructed by radiative decay that is always pointing downwards. That can be seen by the CRM in Figure 11 where the input parameters are a constant $T_e$ but a variable $n_e$. Small absolute differences between experiment and model can be found, they are caused mostly by the strong dependence on $T_e$ as the latter has an experimental uncertainty of about 5%.

The pressure dependence of the Ar(4 s) atom densities is highlighted in Figure 12, where $n(1s)/n_a$ densities close to the launcher are plotted as a function of the pressure and compared to the outcomes of the model. The values of $n_e$ and $T_e$, necessary input for the CRM are from TS measurements and $T_g$ to determine $n_a$ is taken from the present work.

We note that the fractional densities calculated from CRM are in very good agreement with the TDLS data. The steep rise of $n(1s)/n_a$ at the low pressure side is mostly due to the different $T_e$ dependencies of the excitation rate of the Ar(4 s) and the Ar(4 p) levels[33] as it was discussed in the beginning of section IV C.

A note has to be made that $T_e$ is assumed here to obey a Maxwellian distribution. That is questionable[20] as the highest ionization degree in our regime is only around $7 \times 10^{-4}$ at the launcher in low pressure.

## ACKNOWLEDGMENTS

We like to acknowledge the supported by the Dutch Technology Foundation (STW Project Nos. 10497 and 10744) and by the Energy Research Centre of the Netherlands (ECN). We are also in debt to W. A. A. D. Graef for providing and analyzing the CRM.

[1]N. Sadeghi, M. Cheaib, and D. W. Setser, "Comparison of the Ar($^3P_2$) and Ar($^3P_0$) reactions with chlorine and fluorine containing molecules: Propensity for ion-core conservation," J. Chem. Phys. **90**(1), 219–231 (1989).
[2]K. Takechi and M. A. Lieberman, "Effect of Ar addition to an $O_2$ plasma in an inductively coupled, traveling wave driven, large area plasma source: $O_2$/Ar mixture plasma modeling and photoresist etching," J. Appl. Phys. **90**(7), 3205–3211 (2001).
[3]M. E. Bannister and J. L. Cecchi, "Metastable argon beam source using a surface wave sustained plasma," J. Vac. Sci. Technol. A **12**(1),106–113 (1994).
[4]E. R. Ault, "Table-top Ar-$N_2$ laser," Appl. Phys. Lett. **26**(11), 619–620 (1975).
[5]M. Touzeau and D. Pagnon, "Vibrational excitation of $N_2$(C) and $N_2$(B) by metastable argon atoms and the determination of the branching ratio," Chem. Phys. Lett. **53**(2), 355–360 (1978).
[6]F. M. Penning and C. C. J. Addink, "The starting potential of the glow discharge in neon-argon mixtures between large parallel plates: I. Results," Physica **1**(7–12), 1007–1027 (1934).
[7]M. Schulze, A. Yanguas-Gil, A. von Keudell, and P. Awakowicz, "A robust method to measure metastable and resonant state densities from emission spectra in argon and argon-diluted low pressure plasmas," J. Phys. D **41**(6), 065206 (2008).
[8]C. Lao, A. Gamero, A. Sola, Ts. Petrova, E. Benova, G. M. Petrov, and I. Zhelyazkov, "Populations of excited atomic states along argon surface-wave plasma columns at low and intermediate pressures," J. Appl. Phys. **87**(11), 7652–7659 (2000).
[9]G. Cunge, M. Fouchier, M. Brihoum, P. Bodart, M. Touzeau, and N. Sadeghi, "Vacuum UV broad-band absorption spectroscopy: A powerful

diagnostic tool for reactive plasma monitoring," J. Phys. D **44**(12), 122001 (2011).
[10]B. Niermann, I. L. Budunoglu, K. Gürel, M. Böke, F. Ö. Ilday, and J. Winter, "Application of a mode-locked fiber laser for highly time resolved broadband absorption spectroscopy and laser-assisted breakdown on micro-plasmas," J. Phys. D **45**(24), 245202 (2012).
[11]H. Naghshara, S. Sobhanian, S. Khorram, and N. Sadeghi, "Measured density of copper atoms in the ground and metastable states in argon magnetron discharge correlated with the deposition rate," J. Phys. D **44**(2), 025202 (2011).
[12]A. J. M. Buuron, D. K. Otorbaev, M. C. M. van de Sanden, and D. C. Schram, "Absorption spectroscopy on the argon first excited state in an expanding thermal arc plasma," Phys. Rev. E **50**, 1383–1393 (1994).
[13]M. Tadokoro, H. Hirata, N. Nakano, Z. Petrović, and T. Makabe, "Two-dimensional density distribution of metastable atoms in an inductively coupled plasma in Ar," Phys. Rev. E **58**, 7823–7830 (1998).
[14]J. M. de Regt, R. D. Tas, and J. A. M. van der Mullen, "A diode laser absorption study on a 100 MHz argon ICP," J. Phys. D **29**(9), 2404 (1996).
[15]L. Latrasse, N. Sadeghi, A. Lacoste, A. Bès, and J. Pelletier, "Characterization of high density matrix microwave argon plasmas by laser absorption and electric probe diagnostics," J. Phys. D **40**(17), 5177 (2007).
[16]S. G. Belostotskiy, V. M. Donnelly, D. J. Economou, and N. Sadeghi, "Spatially resolved measurements of argon metastable density in a high pressure microdischarge using diode laser absorption spectroscopy," IEEE Trans. Plasma Sci. **37**(6), 852–858 (2009).
[17]J. Jonkers, M. Bakker, and J. J. A. M. van der Mullen, "Absorption measurements on a low-pressure, inductively coupled, argon-mercury discharge for lighting purposes: 1. The gas temperature and argon metastable states density," J. Phys. D **30**(13), 1928 (1997).
[18]M. Moisan and Z. Zakrzewski, "Plasma sources based on the propagation of electromagnetic surface waves," J. Phys. D **24**, 1025–1048 (1991).
[19]J. M. Palomares, E. Iordanova, E. M. van Veldhuizen, L. Baede, A. Gamero, A. Sola, and J. J. A. M. van der Mullen, "Thomson scattering on argon surfatron plasmas at intermediate pressures: Axial profiles of the electron temperature and electron density," Spectrochim. Acta, Part B **65**(3), 225–233 (2010).
[20]E. A. D. Carbone, S. Hübner, M. Jimenez-Diaz, J. M. Palomares, E. Iordanova, W. A. A. D. Graef, A. Gamero, and J. J. A. M. van der Mullen, "Experimental investigation of the electron energy distribution function (EEDF) by Thomson scattering and optical emission spectroscopy," J. Phys. D **45**(47), 475202 (2012).
[21]E. Iordanova, T. Petrova, and E. Benova, "Dominant processes for excited atomic states population in argon surface-wave plasma at low and intermediate pressure," Vacuum **76**(2–3), 413–416 (2004).
[22]W. A. A. D. Graef, "Zero-dimensional models for plasma chemistry," Ph.D. dissertation (Eindhoven University of Technology, The Netherlands, 2012).
[23]S. Hübner, E. Iordanova, J. M. Palomares, E. A. D. Carbone, and J. J. A. M. van der Mullen, "Rayleigh scattering on a microwave surfatron plasma to obtain axial profiles of the atom density and temperature," Eur. Phys. J. **58**(02), 20802-1/10 (2012).
[24]J. M. Palomares, S. Hübner, E. A. D. Carbone, N. de Vries, E. M. van Veldhuizen, A. Sola, A. Gamero, and J. J. A. M. van der Mullen, "Hb stark broadening in cold plasmas with low electron densities calibrated with Thomson scattering," Spectrochim. Acta, Part B **73**(0), 39–47 (2012).
[25]N. Konjević, A. Lesage, J. R. Fuhr, and W. L. Wiese, "Experimental stark widths and shifts for spectral lines of neutral and ionized atoms (a critical review of selected data for the period 1989 through 2000)," J. Phys. Chem. Ref. Data **31**(3), 819–927 (2002).
[26]C. S. Lee, D. M. Camm, and G. H. Copley, "Van der Waals broadening of argon absorption lines," J. Quant. Spectrosc. Radiat. Transf. **15**(3), 211–216 (1975).
[27]N. Sadeghi, private communication (unpublished data).
[28]G. H. Copley and D. M. Camm, "Pressure broadening and shift of argon emission lines," J. Quant. Spectrosc. Radiat. Transf. **14**(9), 899–907 (1974).
[29]R. Engeln, S. Mazouffre, P. Vankan, D. C. Schram, and N. Sadeghi, "Flow dynamics and invasion by background gas of a supersonically expanding thermal plasma," Plasma Sources Sci. Technol. **10**(4), 595 (2001).
[30]E. A. D. Carbone, S. Hübner, J. M. Palomares, and J. J. A. M. van der Mullen, "The radial contraction of argon microwave plasmas studied by Thomson scattering," J. Phys. D **45**(34), 345203 (2012).
[31]N. Sadeghi, "Practical aspects of molecular spectroscopy in plasmas 6. Molecular spectroscopy techniques applied for processing plasma diagnostics," J. Plasma Fus. Res. **80**(9), 767–776 (2004).
[32]G. Cunge, R. Ramos, D. Vempaire, M. Touzeau, M. Neijbauer, and N. Sadeghi, "Gas temperature measurement in $CF_4$, $SF_6$, $O_2$, $Cl_2$, and HBr inductively coupled plasmas," J. Vac. Sci. Technol. A **27**(3), 471–478 (2009).
[33]M. Jimenez-Diaz, E. A. D. Carbone, J. van Dijk, and J. J. A. M. van der Mullen, "A two-dimensional plasimo multiphysics model for the plasma-electromagnetic interaction in surface wave discharges: The surfatron source," J. Phys. D **45**(33), 335204 (2012).
[34]S. Hübner, J. M. Palomares, E. A. D. Carbone, and J. J. A. M. van der Mullen, "A power pulsed low-pressure argon microwave plasma investigated by Thomson scattering: Evidence for molecular assisted recombination," J. Phys. D **45**(5), 055203 (2012).
[35]B. Bakowski, G. Hancock, R. Peverall, S. E. Prince, G. A. D. Ritchie, and L. J. Thornton, "Diode laser measurements of the ar $3p^5$ 4s excited states in an inductively coupled RF plasma," J. Phys. D **38**(16), 2769 (2005).
[36]A. Kramida, Yu. Ralchenko, J. Reader, and NIST ASD Team, NIST Atomic Spectra Database (ver. 5.0), National Institute of Standards and Technology, Gaithersburg, MD, 2013, available at http://physics.nist.gov/asd.
[37]J. J. A. M. van der Mullen, "Excitation equilibria in plasmas: A classification," Phys. Rep. **191**, 109–220 (1990).